



A microscopy study of the effect of heat treatment on the structure and properties of anodised TiO₂ nanotubes

A. Jaroenworarluck^a, D. Regonini^b, C.R. Bowen^b, R. Stevens^{b,*}

^a National Metal and Materials Technology Center, 114 Thailand Science Park, Paholyothin Rd., Klong Luang, Pathumthani 12120, Thailand

^b Materials Research Centre, Department of Mechanical Engineering, University of Bath, Claverton Down Road, Bath BA2 7AY, UK

ARTICLE INFO

Article history:

Received 24 July 2009

Received in revised form 22 September 2009

Accepted 22 September 2009

Available online 1 October 2009

Keywords:

Titanium oxide

Nanotubes

Heat treatment

Phase change

Electron microscopy

ABSTRACT

Titanium oxide (TiO₂) nanotubes prepared by anodisation of titanium in an aqueous electrolyte and glycerol have been heat treated in the temperature range 200–600 °C to control the conversion of the amorphous structure to nano-crystalline anatase and rutile. The phase changes have been monitored and observed at lower temperatures (100 °C or more) than previously reported. The sensitivity of the different techniques, each of which depends on the size of the crystalline phase, can explain the discrepancy with previous results. Transmission electron microscopy (TEM) has shown the phase changes which have occurred and which have been reported in an earlier publication; phenomena such as the collapse of the structures are explained. The TEM results are consistent with the Raman and XRD data, apart from the transformation temperatures, and also shed light on the nature of an amorphous phase found on the surfaces of the nanotubes.

© 2009 Elsevier B.V. All rights reserved.

1. Introduction

Titanium oxide (TiO₂) nanotubes are readily formed by anodisation of titanium metal under the appropriate conditions (voltage, composition of electrolyte, etc.) [1,2]. Development of the nanotubes has been driven by a number of possible applications [3–5]. Earlier studies have shown that the heat treatment of agglomerates of an amorphous TiO₂ hydroxide gel [6] in the nanotubes produces a series of phase changes, eventually developing rutile as the stable phase after heat treatment above ~500 °C. The exact temperature depends on the source and preparation history of the nanotubes [2] and the behaviour appears to be dependent on the interface with the titanium metal, which is believed to act as a nucleation aid [2]. The length of the nanotubes can be controlled [7] and the individual variables involved have been reported [8] towards the fabrication of nanostructures and even nanowires [9].

In the present work we have examined the structure of the anodised film, which has been heat treated after detachment from the titanium substrate and it thus does not rely on this nucleation aid of the titanium–titanium oxide interfacial structures or stresses. A further difference lies in the high surface area of the titania, due to the morphology of the nanotubes and thus the high

surface energy of the anodised film even compared to an annealed TiO₂ gel powder. Apart from the recrystallisation and growth of the nano-grains, the effective surface area is relatively stable until the collapse of the anodised nanotubes on annealing at temperatures above 600 °C, which has been demonstrated in earlier work, using scanning electron microscopy [10]. In order to understand the underlying phenomena, electron microscopy of the as-received and annealed structures has been undertaken using selected area diffraction and lattice imaging to aid identification of the phases present. Comparisons are also made with Raman and X-ray photoelectron spectroscopy (XPS) on the same samples, presented in an earlier publication.

2. Experimental techniques

A commercially pure (99.6%) titanium sheet (0.5 mm thick) was used as an electrode/substrate to be anodised. Anodising was performed by applying a sweep rate of 100 mV/s to 20 V and then held at 20 V for different times, up to 5 h. The process could be interrupted before (after 30 s) or at the end of the sweep (200 s) in order to investigate the early stages of the growth. Using a Teflon electrochemical cell, 0.7 cm² of the metal surface was exposed to the electrolyte (1 M Na₂SO₄ + 0.5 wt.% of NaF) at the anode, while platinum mesh was used as a counter electrode (cathode). The electrolyte temperature was maintained at 20 °C. The electrolyte was slightly stirred during the experiment and both a water-based electrolyte and organic-based electrolyte used to control the

* Corresponding author. Tel.: +44 1225 386549; fax: +44 1225 386928.
E-mail address: r.stevens@bath.or.uk (R. Stevens).

length of the tubes. After anodisation the nanotube films were annealed in air, at 200 °C, 300 °C, 400 °C, 500 °C, 550 °C, and 600 °C for the nanotubes grown in aqueous NaF/Na₂SO₄ and at 450 °C and 500 °C for the nanotubes grown in glycerol. Since both nanotubes grown in aqueous- or glycerol-based electrolyte exhibited a similar response to heat treatment, results are presented mainly for nanotubes grown in aqueous NaF/Na₂SO₄.

The anodised specimens were first examined using SEM and more extensively at a significantly higher magnification using transmission electron microscopy. The TEM samples were prepared by mechanically detaching portions of the oxide film from the metal substrate, mounting the small pieces between a double layer 200 mesh copper grid and observing them directly at 120 kV or 200 kV.

X-ray diffraction (XRD) has been used to follow the crystallisation of the titania film during heat treatment to provide a useful comparison with the Raman technique reported earlier. Morphological and microstructural changes promoted by annealing have been monitored by both scanning electron microscopy (SEM) and transmission electron microscopy (TEM). High resolution TEM (HRTEM) has also been used to support the Raman observations and to determine the crystal phase of the titanium dioxide after the heat treatment.

Two different TEM instruments have been used to characterise the samples. Standard morphological investigations have been possible using a JEOL JEM1200 machine, which is equipped with a tungsten filament and operates within a voltage range 40–120 kV. High resolution images and characterisation of the early stages of the process have been performed (operating at 200 kV) using a JEOL JEM2010 equipped with a LaB₆ electron and capable of operating at a voltage of 80–200 kV. The ability to remove the anodic layer from the metallic substrate following mechanical cracking of the specimen facilitated the preparation of the TEM

samples. Thin sections of material were detached from the anodic film and directly mounted in a double layer 200 mesh copper grid.

SEM characterisation was undertaken with a JEOL JSM6480LV (low vacuum) SEM and a JEOL JSM6310. Measurements have been performed using a voltage within the range 10–30 kV, operating with a working distance in the range 8–10 mm for top view imaging and 15–18 mm for cross-sectional view (tilted samples). At a higher voltage the spherical aberration is reduced allowing higher resolution, however the interaction volume is also extended at a higher voltages and more interactions can also result in a loss of resolution; therefore, a compromise had to be achieved. When a specimen is non-conductive a negative charge from the electron beam tends to accumulate on the surface of the specimen, drastically affecting the final image of the sample. For this reason, anodised TiO₂ nanotubes analysed with the instruments mentioned above, were coated with a thin layer (few nm) of gold, using an ion sputtering device (Edwards Sputter Coater S150B), to eliminate electrostatic charging of the samples.

3. Results and discussion

3.1. SEM evaluation of morphology changes promoted by annealing

This first section is based on SEM evaluation of the morphology changes and stability of anodised TiO₂ grown in aqueous Na₂SO₄/NaF and annealed in air. No significant changes in morphology are observed up to 500 °C, as can be seen from SEM micrographs shown in Fig. 1(a) and (b), which correspond to samples annealed at 400 °C and 500 °C, respectively. It appears that the nanotubes partially collapse after annealing at 550 °C, Fig. 1(c), with some of the oxide rings which build up the nanotubes beginning to sinter together. With a further increase in temperature, the sintering process proceeds to the point where nanotubes are no longer

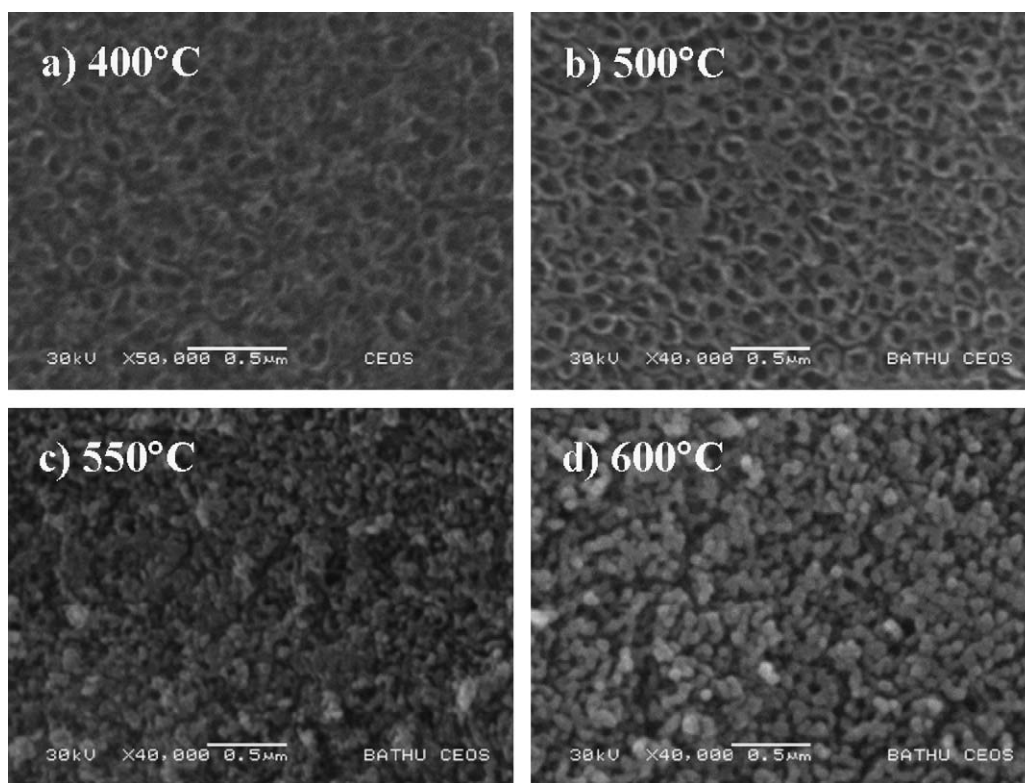


Fig. 1. SEM micrographs of the top of anodised TiO₂ grown in an aqueous Na₂SO₄/NaF electrolyte and annealed at a different temperature. It can be seen that the tubular structure is well preserved at 400 °C (a) and 500 °C (b) while it collapses partially at 550 °C (c). The tubular structure is completely removed at 600 °C (d), where nanoparticles sinter together.

observed at 600 °C, as can be seen in Fig. 1(d). From the SEM images, it is not possible to establish whether the collapse of the anodised nanostructure is related to the formation of rutile, observed at 550–600 °C by Raman. In their previous studies, Grimes and colleagues [2] explained the collapse as the consequence of rutile protrusions emerging from the interface metal/metal oxide into the anodic film following oxidation of substrate at 580 °C and higher temperatures. These protrusions are not observed here using SEM; it should be noted that the annealed specimens in this work have tube lengths of approximately 1.5 μm (while it was 0.5 μm in Grimes study) and this may hide their view on SEM top view images. Certainly at 550 °C the structure is beginning to collapse and particles sinter together. However, it was important to observe the stability of the tubes up to 550 °C as this allows investigation of their performances in dye sensitised solar cells, where anatase is the preferred phase [11,12]. Identical observations were made for tubes grown in glycerol, with the tubes stable up to 500 °C. It should be noted that the very high surface areas of the system together with the presence of an amorphous phase and F⁻ ions, which reduce the melting point of the phase, provide ideal conditions for sintering by means of a liquid phase.

3.2. TEM observation of nanotubes

Detailed information on the morphology and phase changes promoted by annealing of TiO₂ tubes has been provided by TEM examination. For example, using Raman and SEM, it has not been possible to clarify the location of the different crystal phases within the anodic film after the annealing process. The microstructure observed for samples anodised in an aqueous Na₂SO₄/NaF electrolyte and annealed within a temperature range 200–600 °C have been observed. The specimens did not undergo any thinning process (such as PIPS), since this is capable of promoting localised crystallisation due to the ion bombardment. Samples were prepared by detaching the film from the titanium metal substrate and mounting the oxide film onto copper grids. In some cases it has been possible to estimate the lattice spacing of the microcrystals directly from TEM micrographs and compare these with values reported for different polymorphs (anatase and rutile) of titanium dioxide [13]. However due to the size of the crystals there is some potential for systematic errors.

3.2.1. As-prepared nanotubes (no heat treatment)

Previously reported TEM analysis of as-prepared nanotubes shows the structure to consist of very fine grains of anatase distributed in an amorphous matrix [14]. The crystallites tend to form in the more dense arms of the coral-like structure that develops as the pores start to link up to form tubular structures [14]. The presence of crystals may be related to local dielectric breakdown occurring within small section of the film during the growth process or to localised heating caused during the specimen preparation, since the samples did not undergo any form of ion bombardment prior to examination in the TEM.

3.2.2. Microstructure after heat treatment

3.2.2.1. Structure after heat treating at 200 °C. The porous network is clearly visible in the sample annealed at 200 °C as shown by the TEM micrograph in Fig. 2. It is interesting to note that the anodic film has two distinctive types of diffraction pattern. At first, the sample exhibits diffuse 360° overlapping rings typical of an amorphous material, as can be seen from the inset of Fig. 2(a). However, a close inspection of one of the oxide arms composing the network reveals the presence of crystalline areas, with a very clear diffraction contrast, as in Fig. 2 (b) and the corresponding

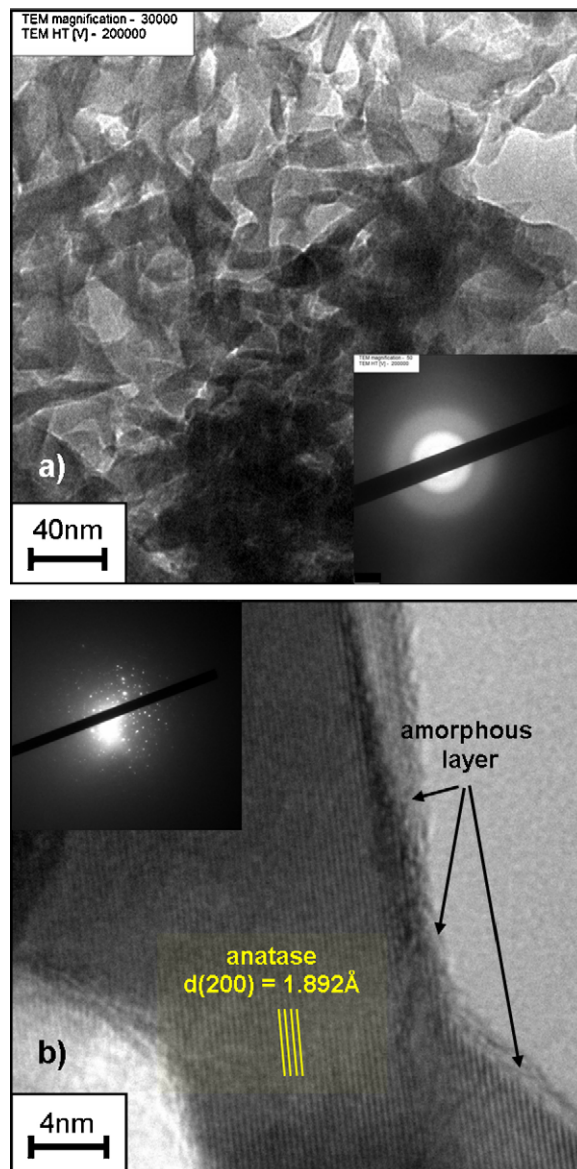


Fig. 2. TEM image of the anodic film after annealing at 200 °C and the corresponding diffraction pattern (inset), showing the presence of an amorphous phase (a). Crystalline anatase is detected by lattice imaging and in the inset electron diffraction pattern (b).

inset. The presence of crystals was not detected using Raman spectroscopy, since the crystalline agglomerates are well dispersed in an amorphous matrix. The lattice spacing in Fig. 2(b) has been measured to be 1.89 Å, which would correspond to the anatase (2 0 0) plane, $d_{(2\ 0\ 0)} = 1.892$ Å. It is of interest that the outer surface of the oxide structure is covered by an amorphous layer which is visible on the free surfaces of the arms of the oxide nanotube. XPS analysis [15] indicates that the fluorine concentration drops from 3.8 at.% in the as-prepared nanotubes to 1 at.% in nanotubes annealed at 300 °C. It is inferred that this sample, annealed at 200 °C, is likely to have a fluorine concentration between these two values, but it is difficult to establish whether this outer amorphous layer of the oxide contains the fluorine contaminant or not. Another possible but less likely source of this amorphous layer could be the carbon organics introduced during the cleaning with isopropyl alcohol, as XPS shows this carbon rich layer is not completely removed on annealing.

3.2.2.2. Structure after heating at 300 °C. The sample annealed at 300 °C clearly shows the three-dimensional structure of the anodised film, Fig. 3(a) and (b), made up of interlocked oxide arms of different diameters and thicknesses. The film is crystalline, as indicated by the diffraction pattern, inset of Fig. 3(a), and this is confirmed by Raman spectroscopy. At a higher magnification, further details of the structure can be resolved. For example in Fig. 4(a) it is possible to identify the phase from the d -spacings of the lattice images. The periodic spacing, $d_{(2\ 0\ 0)} = 1.892$ Å, corresponds to anatase $d(2\ 0\ 0)$. Similar observations can be drawn from the TEM image in Fig. 4(b). The micrograph also shows the presence of other d -spacings, which cannot be easily resolved, but are likely to be due to anatase on the basis of the Raman spectra [15]. Due to the overlapping of different crystals, a rotation Moiré pattern is also observed in the image [16].

Further microstructural information is provided in the micrograph in Fig. 4(c). It would appear as the interior of the arms of the oxide rings are crystalline with the grain boundaries and tri-points free of a second phase. However, as it will be shown in the following sections for samples annealed at higher temperature (400–600 °C), an amorphous phase is present in the outer layer of the oxide and the complete crystallisation observed here may not be representative.

3.2.2.3. Structure after heating at 400 °C. In the well crystallised structure obtained at 400 °C, Fig. 5(a) and its inset, the porous nature of the macrostructure is still clearly visible, in agreement with the SEM results. The three-dimensional structure of the network is well delineated and in certain regions the consistent dark contrast indicates crystallographic continuity. Indeed the recrystallisation behaviour can lead to long sections of the nanotube to have the same orientation along its length. Should these sections be of the $(1\ 0\ 0)$ and the surface energy of the $[1\ 0\ 0]$ be high, then this could account for the cubic arrays reported by Shankar et al. [17], these forming to reduce the overall free energy of the system. An amorphous layer can also be seen at the edges of the grains and on the oxide structure, Fig. 5(b). XPS [15] shows the presence of fluorine ions after heating at 400 °C but the data needs to be treated with care since the total fluorine containing species concentration measured was below 1 at.% at 400 °C. Clearly with such small sections and small dimensions the distribution of fluorine ions is unlikely to be uniform and some differences in the analytical concentrations and the sensitivity is to be expected.

The micrograph, Fig. 5(b), is complex and is characterised by several different overlapping crystals generating Moiré patterns. Nevertheless it is still possible to discriminate between certain of the d -spacings generated from the specimen, particularly those relative to the anatase planes $(2\ 0\ 0)$ and $(1\ 0\ 1)$, respectively, $d_{(2\ 0\ 0)} = 1.892$ Å and $d_{(1\ 0\ 1)} = 3.52$ Å. There is some evidence of an amorphous layer remaining between the individual particles and also at the tri-points of the grains.

3.2.2.4. Structure after heating at 500 °C. The structure is clearly changing shape during heating at 500 °C, with the oxide segments and cavities/voids becoming generally more angular, the process driven by an overall reduction of surface energy. This behaviour is clearly illustrated by the TEM micrograph in Fig. 6(a). An outer amorphous layer is still present; this is shown in Fig. 6(b). It has not been possible to determine the phases present from the d -spacing of the crystals observed in Fig. 6(b) as the calculated d -spacings were in the range 1.68–1.71 Å and this can be attributed either to rutile or anatase. Raman spectroscopy was used on a specimen annealed at 500 °C and the rutile crystal phase was detected in the anodic layer indicating transformation from the anatase had taken place. It is not possible to establish whether the morphological changes observed, with the oxide segments becoming more angular, are related to the formation of rutile crystals. In any event the driving force for morphological shape change to the structure will be the overall reduction in surface energy. The presence of an amorphous film on the surface will clearly affect the surface energy, aid the movement of ionic species and hence speed the changes in morphology of the structure.

3.2.2.5. Heated at 550 °C. Fig. 7(a) shows that the change in morphology continues to take place and modifies the structure. The sample is undergoing densification with the removal of most of the void regions between the arms of the structure, the whole structure becoming consolidated. At increasing magnification, Fig. 7(b) and (c), the individual grains can still be seen to have an amorphous film on the surface, which is present even after the 550 °C heat treatment. The shape of the grains is changing, the equiaxed grains becoming rectangular and elongated with greatly increased aspect ratios, Fig. 7a.

3.2.2.6. Heated at 600 °C. At 600 °C the rate of change is higher still and the TiO₂ structure densifies significantly, the structure of the

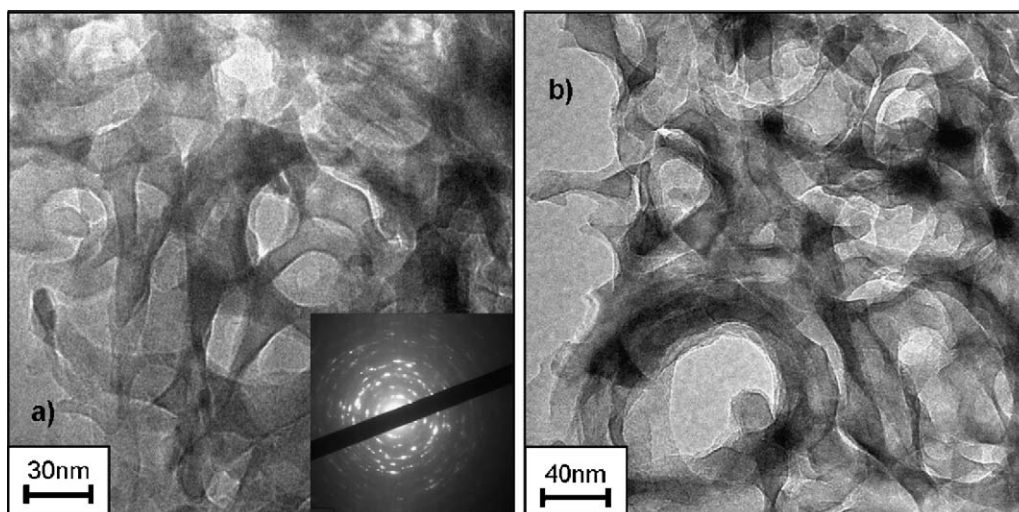


Fig. 3. TEM micrographs taken from anodised TiO₂ nanotubes annealed at 300 °C. The three-dimensional network of oxide rings and cavities is crystalline as suggested by the corresponded diffraction pattern in the inset (a). Further details on the structure are visible in (b).

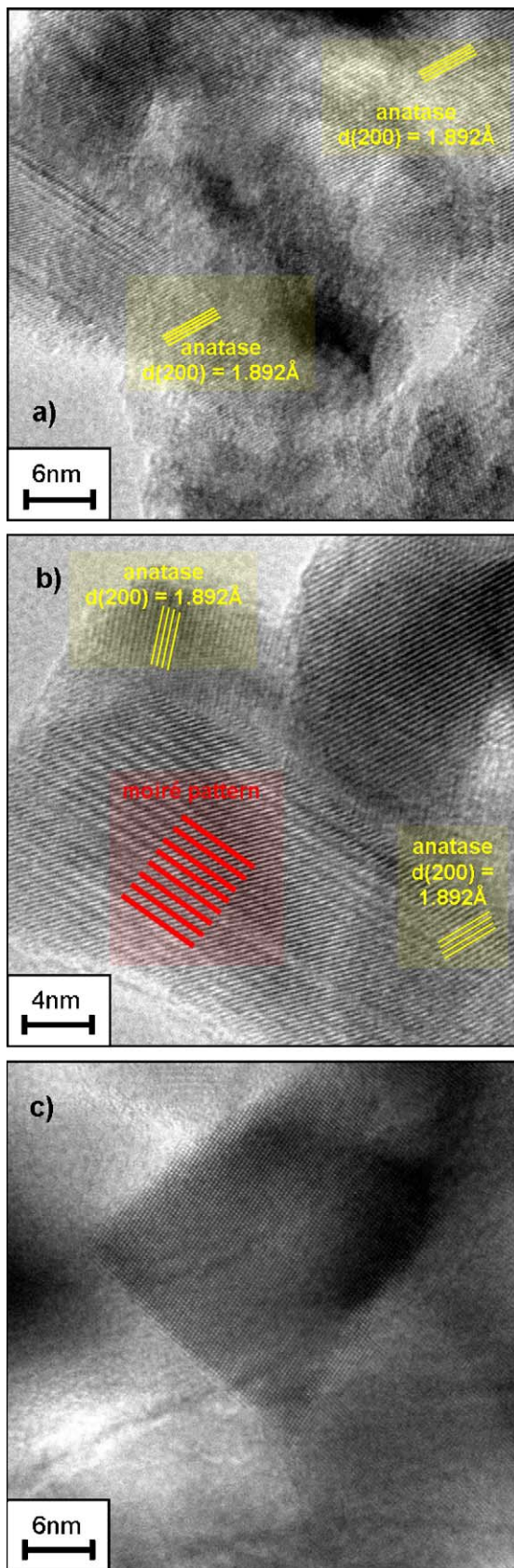


Fig. 4. Details of the crystalline microstructure of anodised TiO₂ nanotubes annealed at 300 °C showing the presence of anatase (a) and (b). It would appear that the structure is fully crystalline (c).

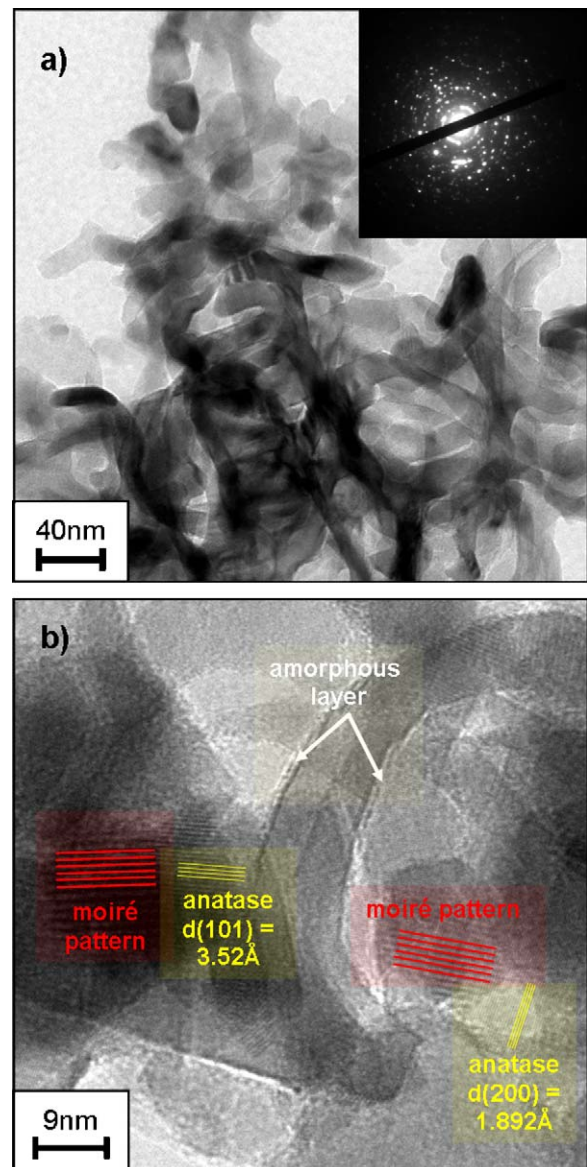


Fig. 5. TEM images of anodised TiO₂ nanotubes annealed at 400 °C. The porous network typical of the structure (a) and the crystallinity in the oxide rings showing the presence of anatase and of an amorphous layer at the crystallite surfaces (b).

nanotubes breaking down as the segments of the titania rings densify and consolidate, Fig. 8(a). The crystals again change shape and are now equiaxed rather than elongated. The fine grain size and hence high surface area of the structure makes the tubes prone to undergo solid state sintering, especially if there is an amorphous phase present which can induce liquid phase sintering. The presence of fluorine ions can significantly reduce the temperature for liquid formation and has been observed in detail for the alumina system [18]. The voids have all but disappeared and the remaining amorphous material, previously coating the free surface of exposed crystals has been redistributed at grain boundaries and tri-points within the structure rather than have remained on the free surfaces, as shown in Fig. 8(b) and (c).

It is interesting that the lattice images showing the d-spacings of anatase are commonly found, Fig. 8(c), whereas it was not possible to identify any contrast images due to rutile planes, even though rutile is the major phase present in the Raman spectrum registered after heating at 600 °C. An explanation of this anomaly is

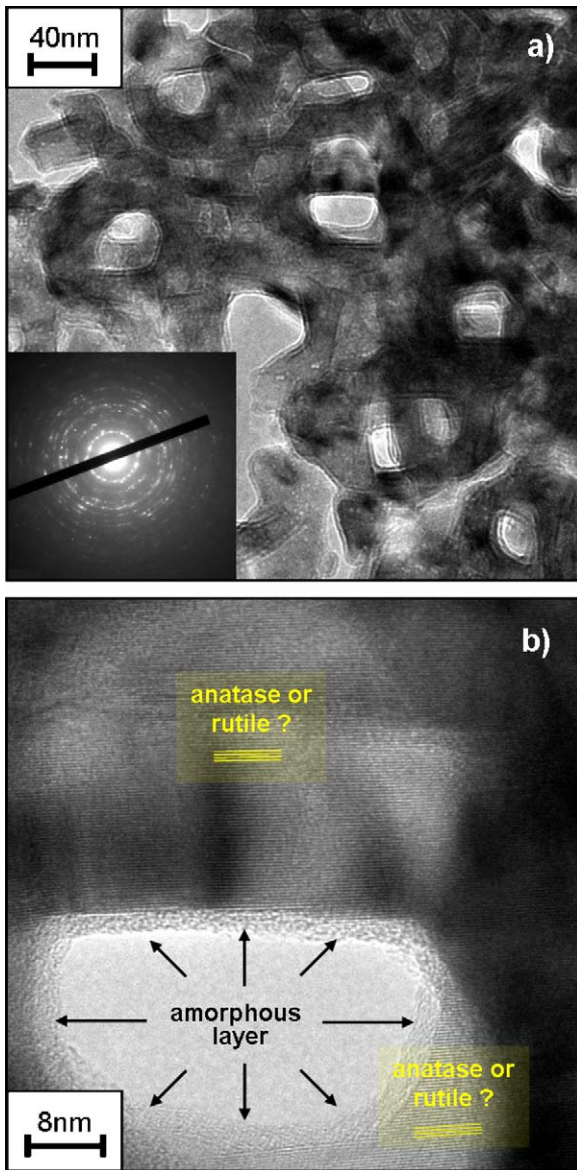


Fig. 6. TEM images of anodised TiO₂ nanotube walls annealed at 500 °C. Reshaping of the oxide segments and the cavities which become more square and angular (a) and anatase crystals in the anodic structure, which still is characterised by an outer amorphous layer (b).

not immediately obvious, the absence of rutile crystals in the anodic structures would suggest, as also suggested by Grimes and colleagues [2], that rutile mainly develops from the metallic substrate, i.e., is nucleated at the titanium/titanium dioxide interface. Since the TEM specimens examined here were prepared from sections of the anodic film detached from the substrate and then heat treated, i.e., in the absence of a metal oxide interface, the rutile crystals may have not been detected by TEM simply because they had not formed in the anodic film as they were unable to nucleate and develop as they would from a metal/metal oxide interface. A further consideration is the very small dimension of the thickness of the films. There is a very large amount of free surface and should the rutile surface energy be higher than that of the anatase phase then crystallisation of the anatase phase would be encouraged. This would support and consolidate the argument made by Grimes and colleagues to this effect. Not all the interfaces have an amorphous layer, indeed some are clean and show close correspondence of lattice images with adjacent grains at the grain

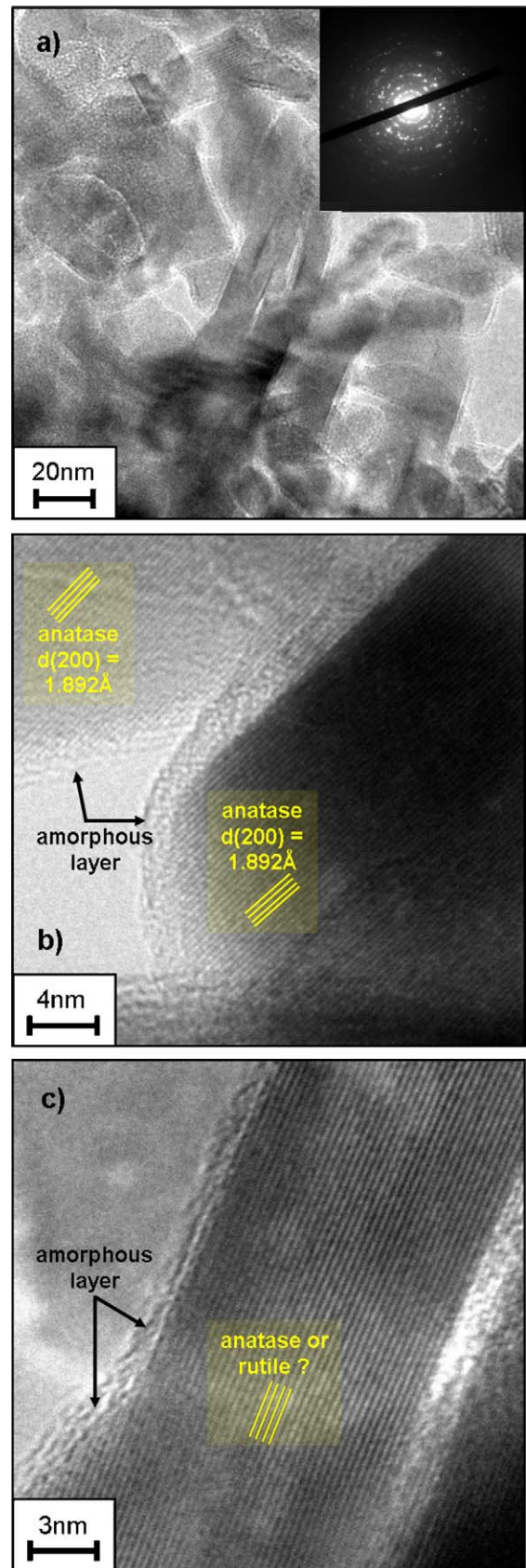


Fig. 7. TEM images of anodised TiO₂ nanotubes annealed at 550 °C. The individual grains have sintered together and the porosity of the structure is decreased. Recrystallisation has taken place resulting in high aspect ratio crystals (a). Analysis of the structure again reveals the presence of anatase and of an amorphous layer on free surfaces (b and c).

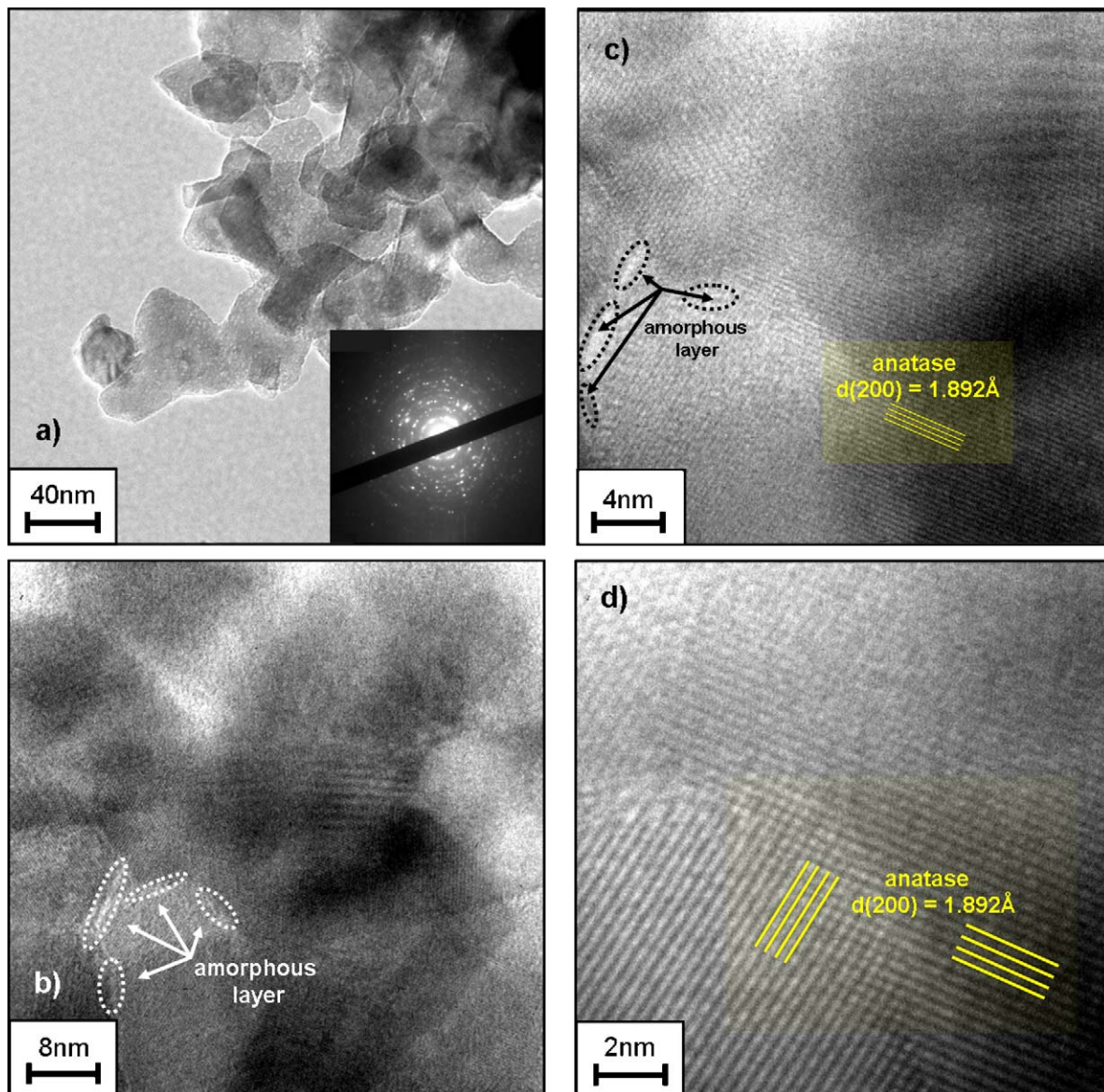


Fig. 8. TEM images of anodised TiO₂ nanotubes annealed at 600 °C. The tubular network no longer exists (a) as the particles have clearly sintered together (b). From the structure the lattice images it is possible to distinguish anatase crystal (c and d).

boundary, Fig. 8(d). Again the d -spacings that are imaged are typical of the anatase (2 0 0) plane, $d_{(2\ 0\ 0)} = 1.892 \text{ \AA}$ and would only be seen in very thin sections of crystal.

4. Conclusions

In summary from the investigation on the effect of thermal treatment on the morphology, crystallinity and composition of the anodic TiO₂ nanotubes, it can be concluded that:

- (i) The nanotubes are stable in an air atmosphere up to 550 °C. When heat treated at a higher temperature (600 °C), sintering of the nanoparticles dominates, densification takes place and the nanotube morphology degrades, aided by the very high surface area and the amorphous film containing fluorine, as observed by SEM and TEM. Removal of pores takes place by densification by a liquid phase sintering mechanism.
- (ii) The nanotubes are clearly made up of aligned segments which are joined at their periphery. The structural arms are interconnected in three-dimensions to form a network which evolves to form a tubular structure. Preferred orientation of the crystals along the length of the tubes occurs.
- (iii) HRTEM analysis shows it is possible to convert the nanotubes from amorphous to anatase and the conversion takes place at around 300 °C, lower than previously reported.
- (iv) At higher temperature rutile appears (500–550 °C) and becomes the dominant phase (600 °C). Rutile d -spacings are not detected from HRTEM of specimens which were prepared by detaching sections of the anodic film from the metallic substrate and then heat treated. This strongly supports the suggestion of Grimes's team that rutile mainly develops at the metal oxide interface and not independently as part of the anodic film.
- (v) After annealing at 550–600 °C, an amorphous outer layer can still be observed by TEM both on the surface of and at the interfaces of the crystallites which form the structure of the titanium oxide segments which make up the tubes. The presence of this amorphous phase would enhance sintering, densification. Finally it results in the collapse of the original structure with increasing temperature and recrystallisation of the grain structure.

Acknowledgement

The authors wish to acknowledge the support of MTEC under Project No. MT-B-48-CER-07-190-I.

References

- [1] G.K. Mor, O.K. Varghese, M. Paulose, K. Shankar, C.A. Grimes, *Sol. Energy Mater. Sol. Cells* 90 (2006) 2011.
- [2] O.K. Varghese, D. Gong, M. Paulose, C.A. Grimes, E.C. Dickey, *J. Mater. Res.* 18 (2003) 156.
- [3] G.K. Mor, K. Shankar, M. Paulose, O.K. Varghese, C.A. Grimes, *Nano Lett.* 6 (2006) 215.
- [4] S.P. Albu, A. Ghicov, J.M. Macak, R. Hahn, P. Schmuki, *Nano Lett.* 7 (2007) 1286.
- [5] G.K. Mor, H.E. Prakasam, O.K. Varghese, K. Shankar, C.A. Grimes, *Nano Lett.* 7 (2007) 2356.
- [6] Y.Z. Huang, D.J. Blackwood, *Electrochim. Acta* 51 (2005) 1099.
- [7] J. Wang, Z. Lin, *Chem. Mater.* 20 (2008) 1257.
- [8] J. Wang, L. Zhao, V.S.Y. Lin, Z. Lin, *J. Mater. Chem.* 19 (2009) 382.
- [9] J. Wang, Z. Lin, *J. Phys. Chem. C* 113 (2009) 4026.
- [10] D. Regonini, C.R. Bowen, R. Stevens, D. Allsopp, A. Jaroenworarluck, *Phys. Status Solidi. A* 204 (2007) 1814.
- [11] H. Tang, K. Prasad, R. Sanjines, P.E. Schmid, F. Levi, *J. Appl. Phys.* 75 (1994) 2042.
- [12] N.-G. Park, J. Van de Lagemaat, A.J. Frank, *J. Phys. Chem. B* 104 (2000) 8989.
- [13] Data taken from the Powder Diffraction File (PDF) from International Centre for Diffraction Data (ICDD), previously known as Joint Committee on Powder Diffraction Standards (JCPDS).
- [14] A. Jaroenworarluck, D. Regonini, C.R. Bowen, R. Stevens, *J. Mater. Res.* 23 (2008) 2116.
- [15] D. Regonini, A. Jaroenworarluck, C.R. Bowen, R. Stevens, *Surf. Interface. Anal.*, in press.
- [16] P.B. Hirsch, A. Howie, R.B. Nicholson, D.W. Pashley, M.J. Whelan, *Electron Microscopy of Thin Crystals*, Butterworths & Co. Ltd., London, 1965.
- [17] K. Shankar, M. Paulose, G.K. Mor, O.K. Varghese, C.A. Grimes, *J. Phys. D* 38 (2005) 3543.
- [18] I. Bennett, R. Stevens, *Br. Ceram. Trans.* 97 (1998) 117.